CrystEngComm

Accepted Manuscript

ROYAL SOCIETY OF CHEMISTRY

www.rsc.org/crystengcomm

Cite this: DOI: 10.1039/c0xx00000x

www.rsc.org/xxxxxx

ARTICLE TYPE

Yttrium hydroxide fluoride based monodisperse mesocrystals: additive-free synthesis, enhanced fluorescent properties, and potential application in temperature sensing

Xianghong He,[a,b] and Bing Yan*[a]

Received (in XXX, XXX) Xth XXXXXXXXX 20XX, Accepted Xth XXXXXXXXX 20XX
DOI: 10.1039/b000000x

Pure and Eu^{3+}-doped yttrium hydroxide fluoride (YHF) monodisperse mesocrystals were fabricated via an additive-free hydrothermal route. Each of the cantaloupe-like architectures is an assembly of aligned nanorods as the subunit in a side-by-side manner. Eu^{3+}-activated YHF mesocrystals exhibited higher red luminescence and improved efficiency compared to microcrystal counterpart, which is believed to be ascribed to the combined effects including high phase purity, well-defined facets, and highly uniform morphologies. Excellent accuracy in temperature determination by fluorescence measurements was achieved with this red-emitting mesocrystal, thus making it suitable for use as luminescence-based thermometer.

Introduction

As a single-crystalline-like architecture composed of orderly aligned nanoparticles, mesoscopically structured crystals termed as 'mesocrystals' represent a unique, 3D building paradigm for hierarchical assembly.[1] The combination of their subunit alignment, high crystallinity, and easy processing ability due to micrometer size region of the whole architecture ensures the mesocrystals a new possibility for advanced materials design as well as constructing multifunctional materials with remarkable and exciting properties.[2] Therefore, in this decade, significant efforts are made to synthesize or discover mesocrystal systems in a wide range of compositions such as metal oxides,[3] hydroxides,[4] coordination polymers,[5] and metals,[6] as well as inorganic salts including carbonate, phosphate, tungstate, titanate, borate, and sulfide.[7] Nevertheless, the spectrum of known mesocrystals is still quite limited, in which reports on fluorine-containing compound mesocrystallines are few and far between.[8] On the other hand, organic additives are commonly used to bridge and orient the subunits as well as to stabilize (steric or electrosteric stabilization) the primary nanoparticles and to alter the shape of the primary nanoparticles during formation of mesocrystals.[1a,2b,9] Currently, it still remains a big challenge to rationally fabricate highly ordered mesocrystals formed from nonspherical nanoparticles in the absence of any organic additives through a simple route.[2b,2c,3a,3f,3j,6a] Moreover, far less information is available concerning physical and chemical properties (especially the optical properties) arising from the mesocrystal materials.[1g,2a,2c,7g,8a,8b] Although increasing efforts has been put onto transferring mesocrystals into various applications including photocatalysts, gas sensors, electrodes, optoelectronics, biomedical materials, hard templates, energy conversion and storage, and lightweight structural materials,[1e,1f,2b-2d,3a,3c,3e,3g,3j,4,7e,7f] exploring potential applications of the mesocrystal materials is eagerly demanded.

As one important member of UCl_3-typed rare-earth compounds family,[10] yttrium hydroxide fluoride (YHF) with the chemical composition $Y(OH)_{3-x}F_x$ ($0.65 < x < 1.43$) can be obtained through lower temperature hydrothermal treatment.[8a] In addition, it can provide suitable Y^{3+} sites at which trivalent rare-earth elements can be easily substituted without additional charge compensation. Most recently, the development of novel rare-earth nanophosphors has lead to a rebirth of interest in this compound for serving as host crystal for photo-active lanthanide ions due to its broader anion miscibility ranges relative to hydroxide chlorides and hydroxide bromides.[11] However, no effort has been made to reveal the photoluminescent properties and potential application of YHF-based mesocrystals as well as the difference between the mesocrystal and micro-/nano-crystal counterpart. Herein, YHF was employed as a proof-of-concept compound to construct highly ordered mesocrystal from nonspherical nanoparticles and to explore the remarkable optical properties of mesocrystalline materials. The higher quantum yield of Eu^{3+} doped mesocrystal compared to microcrystal counterpart was reported for the first time. Impressively, its temperature-dependent photoluminescent properties established its potential as a self-calibrated luminescent thermometer.

Experimental section

Materials.

Rare-earths (RE) oxides (Y_2O_3, and Eu_2O_3, 99.99%), NaOH (≥ 96.0%), NaF (≥ 98.0%), concentrated nitric acid (HNO_3, ≥ 68.0%), and ethanol (≥ 99.7%) were purchased from Sinopharm Chemical Reagent Co., China. RE oxides were separately dissolved in dilute HNO_3 solution and the residual HNO_3 was

removed by heating and evaporation, resulting in the formation of aqueous solution of corresponding $RE(NO_3)_3{\cdot}xH_2O$. All reagents and solvents were used as received without further purification.

Synthesis.

$Y(OH)_{3-x}F_x$ and Eu^{3+}-doped $Y(OH)_{3-x}F_x$ mesocrystals (YHF:Eu^{3+}) were prepared a simple hydrothermal method. Herein took the synthesis of YHF as an example. $Y(NO_3)_3{\cdot}xH_2O$ aqueous solution (0.20 M, 5.00 mL) was fully mixed with NaF (0.50 M, 3.00 mL) solution under vigorous stirring at room temperature. Thereafter, pH value of the resultant mixing solution was adjusted to ~ 8 by adding proper amount NaOH aqueous solution. After stirring for 15 min, the mixture was transferred to a 25 mL Teflon lined autoclave. The autoclave was placed in a digital temperature-controlled oven and operated at 100 °C for 5 hrs and then was allowed to cool to room temperature naturally. Subsequently, the white precipitate was collected by centrifugation, and washed sequentially with deionized water and ethanol for several times. After drying at 65 °C under dynamic vacuum for 24 hrs, YHF sample was obtained.

YHF:Eu^{3+} microcrystals were prepared by a recently reported procedure with a slight modification.[11a] Briefly, the mixing solution of $Y(NO_3)_3$ (0.95 mmol) and $Eu(NO_3)_3$ (0.05 mmol) was added into $NH_3{\cdot}H_2O$ aqueous solution (1:1, V/V) containing benzoic acid (0.366 g) under vigorous stirring at room temperature. Then, NaF aqueous solution (0.75 M, 4.00 mL) was dropped into the mixture under continuous stirring for 45 min. Finally, the mixture was transferred to a 50 mL Teflon-lined autoclave and heated at 160 °C for 36 hrs. The other procedures are similar to the above mentioned routine for synthesis of mesocrystals.

Characterization.

Powder X-ray diffraction (XRD) patterns of the as-synthesized samples were recorded with a Bruker D8 Advanced X-Ray Diffractometer with Ni filtered Cu Ka radiation (λ = 1.5406 Å) at a voltage of 40 kV and a current of 40 mA. The morphologies of samples were characterized by Field emission scanning electron microscopy (FESEM, Hitachi S4800) and transmission electron microscopy (TEM, JEOL-2100F). The selected area electron diffraction (SAED) patterns and energy-dispersive X-ray spectroscopic (EDX) analysis were acquired using TEM (JEOL-2100F). TEM specimens were prepared by depositing a drop of ethanol solution containing the products onto holey carbon-coated grids. X-ray photon spectroscopy (XPS) was recorded with a RBD upgraded PHI-5000C ESCA system (Perkin Elmer), where the analysis chamber was about 5×10^{-8} Pa and the size of the X-ray spot was 500 μm. All of the spectra were referenced to the C1s binding energy of 284.6 eV. Spectra were analyzed using RBD AugerScan 3.21 software. Infared (IR) spectrum analyses were operated on samples pelletized with KBr powder in the range of 4000−400 cm^{-1} using an infrared Fourier transform spectrophotometer (Nicolet, ZOSX). Temperature-dependent emission spectra and luminescence decay curve were examined by Edinburgh FLS920 phosphorimeter. Photoluminescence (PL) absolute quantum yield of solid state samples were determined employing an integrating sphere (150 mm diameter, $BaSO_4$ coating) from Edinburgh FLS920 phosphorimeter.

Results and discussion

Morphology, chemical composition and phase analysis.

Mesocrystalline YHF was fabricated by hydrothermal reactions of $Y(NO_3)_3$, NaF, and NaOH aqueous solution at 100 °C without any organic additives. After shorter time of reaction, a large amount of cantaloupe-like superstructures was obtained, as shown in Fig. 1. The representative SEM images show that YHF exhibited uniform cantaloupe-like microparticle with the average longitudinal axis of ca. 1.55 μm and horizontal axis of ca. 0.95 μm (Fig. 1a and 1b). Nanorods with diameters of ca. 50 nm were clearly observed not only on the surface but also within the interior of the architecture. These nanorods are aggregated together in a side-by-side manner, indicating that cantaloupe-like architecture was composed of many aligned nanorods as the subunit. A typical TEM image (Fig. 1c) of a single mesocrystal further confirmed that YHF consists of nanosized subunits with sizes of around 50 nm. The selected-area electron diffraction (SAED) pattern (Fig. 1d) exhibits sharp and highly symmetrical spots, revealing its single-crystal-like feature. All together, the above results testified that the cantaloupe-like superstructure YHF is actually a typical mesocrystalline. Moreover, the rough surface and attachment of nanorods in a side-by-side manner, suggest that the YHF mesocrystals resulted from self-assembling of nonspherical nanoparticle subunits rather than the classic crystal growth.[1a,1c,1e,3i]

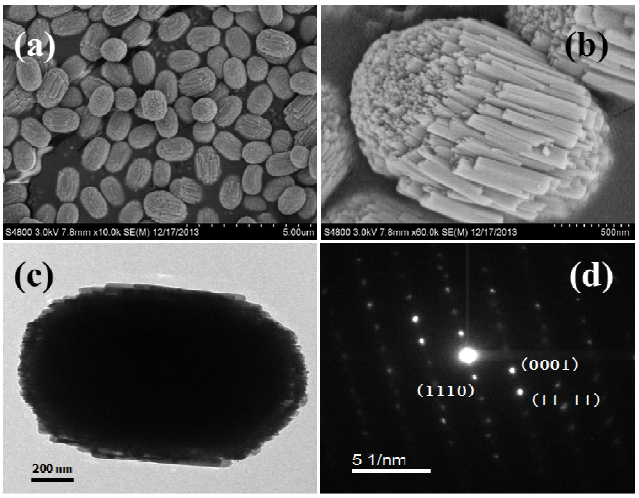

Fig. 1 Low-magnification (a) and high-magnification (b) SEM, (c) TEM images and (d) SAED pattern of YHF mesocrystals.

As depicted in Fig. 2a, the powder X-ray diffraction (XRD) pattern of the as-obtained YHF mesocrystal exhibited sharp and intense peaks indicative of highly crystalline. It agreed well with that of YHF phase (JCPDS flies no.80-2008) with the composition $Y(OH)_{3-x}F_x$ (where x = 1.43), except that reflection peaks of as-synthesized mesocrystal shifted towards higher angle relative to JCPDS data.[10] No trace of other characteristic peaks was observed for impurity phases. Compositional analysis by EDS and XPS (Figs. S1 and S2 of ESI) of these samples indicates that the chemical signatures taken within different parts of the sample are identical and that the as-obtained sample contains Y,

O, and F elements. The atomic ratio of F to Y is calculated to be approximately 1.423: 1, which approaches the feed value of 1.5: 1. In addition, the presence of strong absorption bands at 792 and 599 cm^{-1} as well as intense and sharp peak at 3624 cm^{-1} in IR spectrum (Fig. 2b) evidenced the existence of hydroxyl group (OH) in the resultant mesocrystal compound.[12] Accordingly, the as-obtained YHF mesocrystal can be identified as $Y(OH)_{1.57}F_{1.43}$ phase with hexagonal structure. The calculated lattice constants are as follows: a = 6.085 ± 0.004 Å, c = 3.556 ± 0.002 Å, which is in good agreement with the corresponding values for the bulk hexagonal $Y(OH)_{1.57}F_{1.43}$.

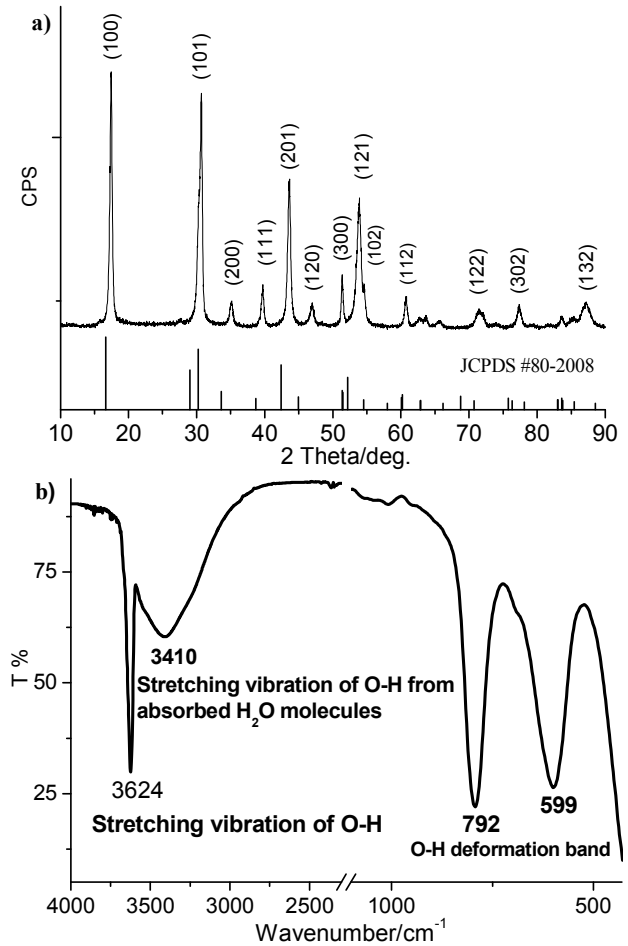

Fig. 2 (a) XRD pattern (the standard data of JCPDS No.80-2008 is shown as a reference), (b) FT-IR spectrum of YHF mesocrystal and the assignment of absorption band.

Room-temperature Photoluminescence Spectroscopy.

Eu^{3+} was *in-situ* introduced into YHF mesocrystal through hydrothermal method under experimental conditions identical with those employed for host samples. XRD patterns of as-obtained YHF:Eu^{3+}(*y* mol%) mesocrystalline phosphors with *y* = 5, 10, and 20 are shown in Fig. 3a. Similar to that of pure YHF mesocrystal, all the diffraction peaks can be readily indexed to $Y(OH)_{3-x}F_x$ phase with hexagonal structure.[10] No peaks from other phases are detected, indicating that the samples are of high purity. With increasing of Eu^{3+} doping content, the reflection peaks are slightly shifted towards smaller angles, which is associated with unit-cell volume expansion due to the substitution of Y^{3+} [Coordination Number (CN) = 6, Ionic Radius (*r*) = 0.90 Å] by the larger Eu^{3+} (CN = 6, *r* = 0.947 Å) in the crystal matrix. This also suggests that Eu^{3+} has been incorporated into host lattices by substituting Y^{3+} sites, which was further verified by the later finding that the sample exhibits red emission after introducing Eu^{3+} ion into YHF host lattice (Fig. 3c).

Fig. 3b shows the SEM images of selected mesocrystalline phosphors with three typical compositions. With the Eu^{3+} concentration increasing from 5 to 20 mol%, the size of the microparticles slightly increased, while the shape remained unchanged. Obviously, each of cantaloupe-like architectures remains a mesocrystal, i.e., an assembly of nanocrystals with a uniform crystallographic orientation, irrespective of the Eu^{3+} doping content.

Fig. 3c displays emission spectra of YHF:Eu^{3+} mesocrystalline phosphors with different Eu^{3+} doping concentration. Upon excitation of 395 nm near UV light (the most effective direct excitation of Eu^{3+} ion, see Fig. S3 of ESI), all the samples exhibited an intense, characteristic luminescence of Eu^{3+} ion including $^5D_0 \rightarrow {}^7F_0$ transition at 580 nm, $^5D_0 \rightarrow {}^7F_1$ transition at 593 nm, $^5D_0 \rightarrow {}^7F_2$ transition at 615 nm, and $^5D_0 \rightarrow {}^7F_4$ transition at 696 nm. The emission intensity of $^5D_0 \rightarrow {}^7F_2$ (electric-dipole) is obviously stronger than that of $^5D_0 \rightarrow {}^7F_1$ (magnetic-dipole) transition. The presence of a single peak due to $^5D_0 \rightarrow {}^7F_0$ transition implies that Eu^{3+} ion occupies a single site in host lattices.[12d,13a-13g] According to the Judd−Ofelt theory, if Eu^{3+} occupied the sites with inversion symmetry the $^5D_0 \rightarrow {}^7F_1$ magnetic dipole transition will be the dominant ones; otherwise, the $^5D_0 \rightarrow {}^7F_2$ electric dipole transition is the strongest.[12d,13a-13g] Moreover, the integrated intensity ratio of electric-dipole to magnetic-dipole transition (denoted as R/O ratio), also called the asymmetric ratio, can be used to assess the symmetry of local crystal field in the vicinity of Eu^{3+} ion.[13c-13g] Herein, the R/O ratio of the mesocrystal phosphor was calculated to be 2.52, indicating that Eu^{3+} locates at the site without inversion symmetry. In the lattice structure of YHF compounds, Y^{3+} is coordinated by six anions in a corner of the trigonal prism and three anions on the three prism walls.[10] Consequently, it is believed that Eu^{3+} occupied nine-coordinated Y^{3+} site in YHF host matrixes. As exhibited in Fig. 3c, with elevating Eu^{3+} content, the luminescence from Eu^{3+} ion was greatly enhanced, accompanied with the slightly increasing of size of the resultant mesocrystals. The Commission Internationale de L'Eclairage (CIE) chromaticity coordinates for YHF: Eu^{3+}(5 mol%) are calculated to be (*x* = 0.55, *y* = 0.33), located in the red light region (Fig. S4 of ESI).

Vibration Mode and Photoluminescence comparison between mesocrystals and microcrystal counterpart.

In order to reveal the difference of vibration mode and luminescence properties between the mesocrystal and microcrystal counterpart, Eu^{3+}-activated YHF red-emitting microcrystal was selected as the reference. XRD pattern and morphology of YHF:Eu^{3+}(5 mol%) microcrystal are shown in Figs. S5 and S6 of ESI, respectively.

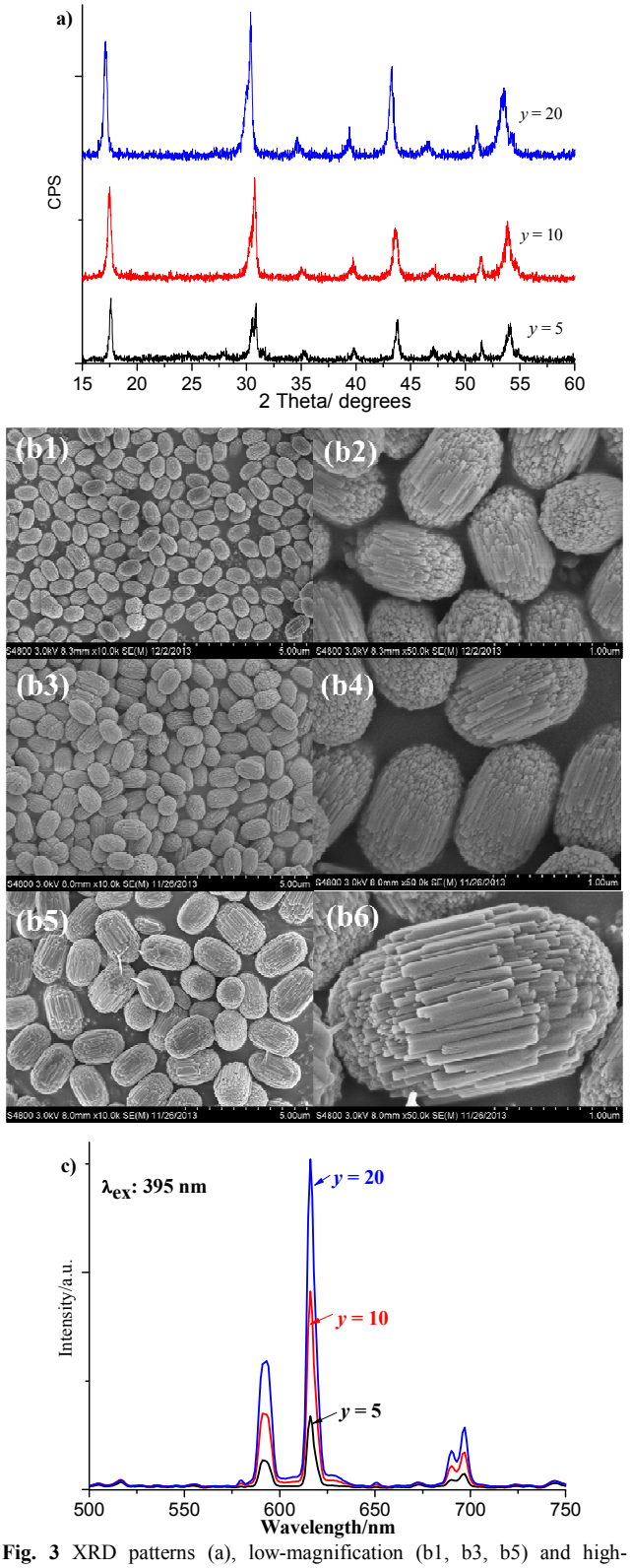

Fig. 3 XRD patterns (a), low-magnification (b1, b3, b5) and high-magnification (b2, b4, b6) SEM images (b) [(b1, b2) $y = 5$; (b3, b4) $y = 10$; (b5, b6) $y = 20$], and emission spectra (c) of Eu^{3+}-activated YHF mesocrystalline phosphors with different Eu^{3+} doping concentration (y mol%).

IR spectrum comparison between the as-synthesized YHF:Eu^{3+} mesocrystal and microcrystal phosphors was presented in Fig. 4a. The stretching vibration of OH group showed similar behavior in both the microcrystal and mesocrystal samples. However, the OH deformation bands observed at 771, and 515 cm^{-1} in the microcrystal have been shifted to 792, and 600 cm^{-1} in mesocrystal, respectively. The shifting towards higher energies is believed to be related to the enhanced hydrogen bonds between the OH group and the F atom, [12a,12c] which may be resulted from the crystallographically alignment of the subunit in mesocrystals. And this phenomenon was the first report in mesocrystalline compounds.

The comparison of photoluminescence behavior between mesocrystal and microcrystal phosphors was given in Figs. 4b, 4c, and 4d, and Table S1 (ESI). As depicted in Fig. 4b, both mesocrystal and microcrystal samples exhibit red emission upon excitation of 395 nm near UV light. The former exhibited much stronger luminescence than that of the latter. The R/O ratio of the microcrystal phosphor was calculated to be 1.87, smaller than that of mesocrystalline phosphor (2.52). Generally, the larger the asymmetric ratio of Eu^{3+}-activated phosphors, the lower the local symmetry.[13c-13g] Herein, the larger R/O ratio for the mesocrystal indicated that a decline of centrosymmetric character of the crystal field around Eu^{3+} ions in lattice.[13f,13g] We speculated that the decline of centrosymmetry is due to the above-mentioned enhanced hydrogen bond between OH group and F atom in YHF based mesocrystallines. The luminescence decay curves for Eu^{3+} ($^5D_0 \rightarrow {}^7F_2$, 615 nm) in YHF:$Eu^{3+}$ mesocrystal and microcrystal samples at room temperature are shown in Figs. 4c and 4d, respectively. All the decay curves can be fitted well by a single-exponential function $I(t) = I_0 \exp(-t/\tau)$, where I_0 is the initial emission intensity at $t = 0$, and τ is the 1/e lifetime of the emission center. The lifetime for the mesocrystal was measured to be about 1.28 ms, longer than that of microcrystal (0.87 ms). Furthermore, the absolute quantum yield (QY) of mesocrystal red-emitting phosphor was determined be 41.5 %, much bigger than that of microcrystal (20.9 %).

Temperature-dependent luminescent behavior.

Considering its higher quantum efficiency, the temperature-dependent PL properties of YHF:Eu^{3+} mesocrystalline were investigated in an attempt to establish its potential as a luminescent thermometer. The emission spectra of YHF:Eu^{3+} mesocrystal in the temperature ranging from 300 K to 500 K are shown in Fig. 5a, and the intensity of $^5D_0 \rightarrow {}^7F_2$ transition (615 nm) is illustrated in Fig. 5b. As expected, the red emission intensity decrease gradually as the temperature increases. The emission intensity decreases by 0.358% per K on increasing temperature from 400 K to 500 K. In other words, the sensitivity is 0.358% per K. The absolute temperature (T) is linearly correlated to normalized emission intensity (I_n) from 400 to 500 K, as revealed in the following equation, $I_n = 1.585 - 0.00358T$. This suggests that YHF:Eu^{3+} mesocrystal is a potentially useful luminescent thermometer in the temperature range from 400 K to 500 K.

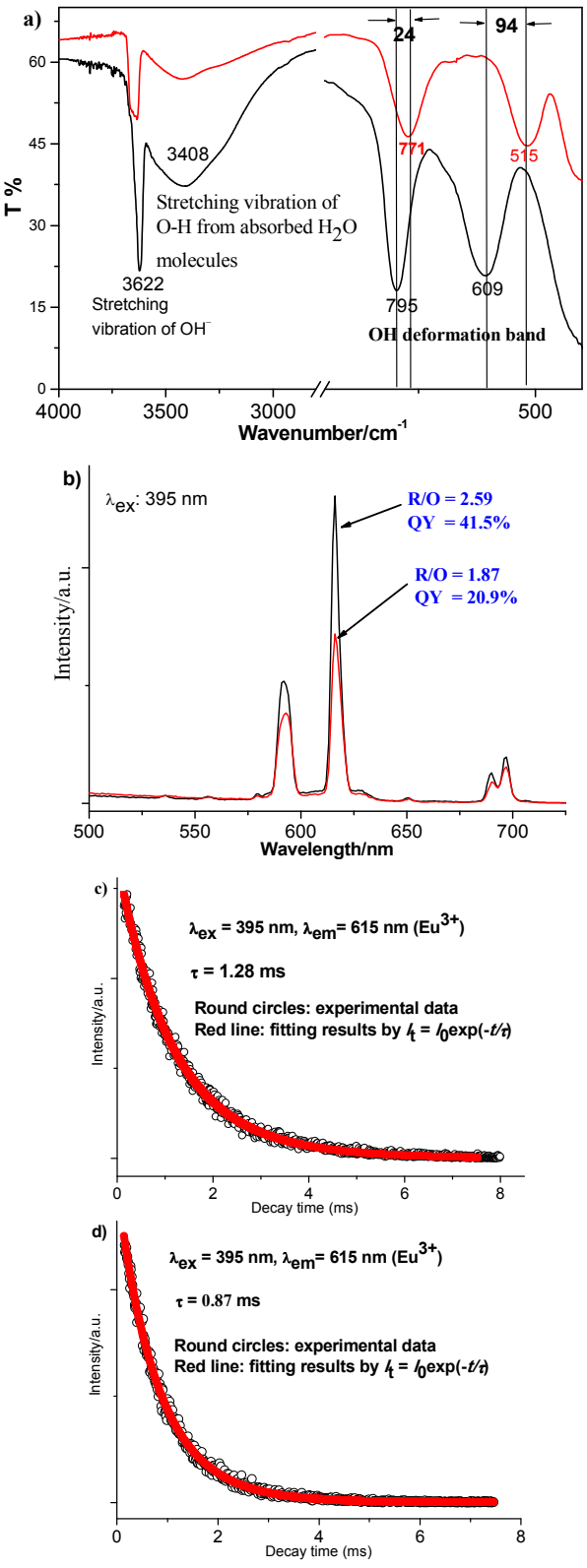

Fig. 4 (a) IR spectra of YHF:Eu^{3+}(5 mol%) microcrystal (upper curve) and mesocrystal (below curve) phosphors (the wavenumber differences of absorption band due to OH deformation vibration modes are marked); (b) emission spectra of as-synthesized YHF:Eu^{3+}(5 mol%) mesocrystal (upper curve) and microcrystal (below curve) phosphors (R/O ratio and QY values are given); luminescence decay profiles of $^5D_0 \rightarrow {}^7F_2$ (615 nm) transition in YHF:Eu^{3+}(5 mol%) mesocrystalline (c) and microcrystal (d) phosphors.

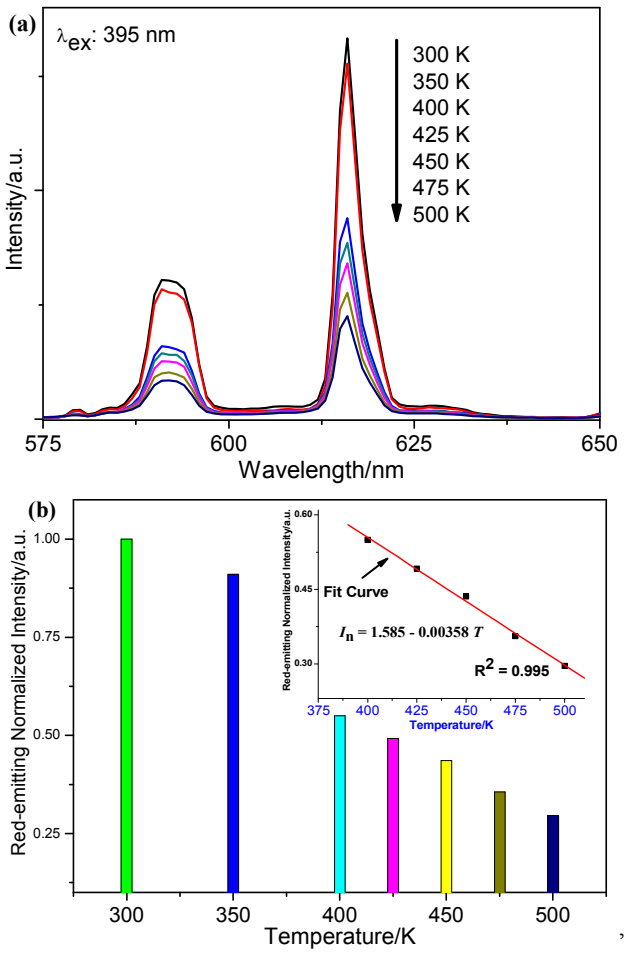

Fig. 5 (a) Emission spectra of Eu^{3+}-activated YHF mesocrystal at various temperatures (300 K – 500 K), (b) Normalized emission intensity at different temperatures (300 K – 500 K) [the inset shows the temperature-dependent intensity and the fitted curve (400 K – 500 K)].

Conclusions

In summary, monodisperse yttrium hydroxide fluoride mesocrystal as well as their Eu^{3+} doped analogue were fabricated by an additive-free hydrothermal reaction of Y^{3+} and F^- with OH^-. The resultant mesocrystals were formed from the self-assemble of nanorods stacking parallel along their *c* axes. Upon *in situ* doping Eu^{3+} into YHF host lattices, Eu^{3+}-activated red-emitting phosphors were obtained. Compared to the microcrystal counterpart, OH deformation absorption bands of the mesocrystals shifted towards higher energies. In addition, Eu^{3+}-activated mesocrystals exhibited enhanced photoluminescent performance, which is believed to be due to the intrinsic single-crystal-like nature including high phase purity and well-defined facets as well as highly uniform morphologies. Especially, it was found that absolute temperature is linearly correlated to normalized red emission intensity of Eu^{3+}-doped YHF mesocrystal from 400 to 500 K. Moreover, such mesocrystal thermometer does not require any additional calibration of luminescence intensity, it is much more instantaneous than the widely explored luminescent solid thermometers.[14] Consequently, it is expected that this YHF based fluorescent mesocrystalline

material can be used as luminescence-based thermometer.

ACKNOWLEDGMENTS

The authors gratefully acknowledge financial support from Natural Science Foundation of China (Grant No. 91122003) and Developing Science Funds of Tongji University.

Notes and references

[a] *Department of Chemistry, Tongji University, Shanghai 200092, China. E-mail: byan@tongji.edu.cn*

[b] *School of Chemistry and Environmental Engineering, Jiangsu University of Technology, Changzhou, Jiangsu 213001, China. E-mail: hexh@jsut.edu.cn*

† Electronic Supplementary Information (ESI) available: Experimental details, EDS, and X-ray photoelectron survey spectra of mesocrystal; Excitation spectrum, and CIE chromaticity diagram for mesocrystalline phosphor; XRD pattern, and SEM image of microcrystal phosphor; Summary of the Asymmetry Ratio, Lifetime, and Quantum Yield. See DOI: 10.1039/b000000x/

1 (*a*) H. Cölfen and M. Antonietti, *Angew. Chem. Int. Ed.*, 2005, **44**, 5576; (*b*) M. Niederberger and H. Cölfen, *Phys. Chem. Chem. Phys.*, 2006, **8**, 3271; (*c*) L. Zhou and P. O'Brien, *Small*, 2008, **4**, 1566; (*d*) R. Q. Song and H. Cölfen, H. *Adv. Mater.*, 2010, **22**, 1301; (*e*) J. X. Fang, B. J. Ding and H. Gleiter, *Chem. Soc. Rev.*, 2011, **40**, 5347; (*f*) L. Zhou and P. O'Brien, *J. Phys. Chem. Lett.*, 2012, **3**, 620.

2 (*a*) M. Distaso, D. Segets, R. Wernet, R. K. Taylor and W. Peukert, *Nanoscale*, 2012, **4**, 864; (*b*) Minwei Xu, Fei Wang, Bingjun Ding, Xiaoping Song and Jixiang Fang, *Chem. Commun.,* 2012, **48**, 2204; (*c*) J. Ye, W. Liu, J. Cai, S. Chen, X. Zhao, H. Zhou and L. Qi, *J. Am. Chem. Soc.*, 2011, **133**, 933; (*d*) X. Yao, X. Liu, T. Liu, K. Wang and L. Lu, *CrystEngComm*, 2013, **15**, 10246.

3 (*a*) T. Tachikawa and T. Majima, *NPG Asia Mater.*, 2014, **6**, e100; (*b*) P. Tartaj and J. M. Amarilla, *Adv. Mater.*, 2011, **23**, 4904; (*c*) S. Deng, V. Tjoa, H. M. Fan, H. R. Tan, D. C. Sayle, M. Olivo, S. Mhaisalkar, J. Wei and C. H. Sow, *J. Am. Chem. Soc.*, 2012, **134**, 4905; (*d*) T. Ikeda, Y. Oaki and H. Imai, *Chem. Asian J.*, 2013, **8**, 2064; (*e*) Y. J. Liu, G. X. Zhu, B. L. Ge, H. Zhou, A. H. Yuan and X. P. Shen, X. P. *CrystEngComm*, 2012, **14**, 6264; (*f*) F. Waltz, G. Wißmann, J. Lippke, A. M. Schneider, H. C. Schwarz, A. Feldhoff, S. Eiden and P. Behrens, *Cryst. Growth Des.*, 2012, **12**, 3066; (*g*) J. Ma, J. Teo, L. Mei, Z. Zhong, Q. Li, T. Wang, X. Duan, J. Lian and W. Zheng, *J. Mater. Chem.*, 2012, **22**, 11694; (*h*) C. Lausser, H. Colfen and M. Antonietti, *ACS Nano*, 2011, **5**, 107; (*i*) M. Zheng, Y. Liu, Y. Xiao, H. Dong, H. Feng, H. Zhang and B. Lei, *ACS Appl. Mater. Interfaces*, 2013, **5**, 12561; (*j*)D. Wang, J. Li, X. Cao, G. Pang and S. Feng, *Chem. Commun.*, 2010, **46**, 7718; (*k*) E. J. W. Crossland, N. Noel, V. Sivaram, T. Leijtens, J. A. Alexander-Webber, and H. J. Snaith, *Nature*, 2013, **495**, 215.

4 L. R. Hou, C. Z. Yuan, L. Yang, L. F. Shen, F. Zhang and X. G. Zhang, *CrystEngComm*, 2011, **13**, 6130.

5 (*a*) M. Hu, S. Furukawa, R. Ohtani, H. Sukegawa, Y. Nemoto, J. Reboul, S. Kitagawa, and Y. Yamauchi, *Angew. Chem. Int. Ed.* 2012, **51**, 984; (*b*) M. Hu, J. Jiang, R. Ji, and Y. Zeng, *CrystEngComm*, 2009, **11**, 2257.

6 (*a*) X. Q. Huang, S. H. Tang, J. Yang, Y. M. Tan and N. F. Zheng, *J. Am. Chem. Soc.*, 2011, **133**, 15946; (*b*) T. Li, H. You, M. Xu, X. Song and J. Fang, *ACS Appl. Mater. Interfaces*, 2012, **4**, 6942; (*c*) J. X. Fang, B. J. Ding and X. P. Song, *Appl. Phys. Lett.*, 2007, **91**, 083108.

7 (*a*) H. D. Yu, D. Yang, D. Wang and M. Y. Han, *Adv. Mater.*, 2010, **22**, 3181; (*b*) R. Q. Song, A. W. Xu, M. Antonietti and H. Cölfen, Angew. Chem. Int. Ed., 2009, **48**, 395; (*c*) J. J. M. Lenders, A. Dey, P. H. H. Bomans, J. Spielmann, M. M. R. M. Hendrix, G. de With, F. C. Meldrum, S. Harder and N. A. J. M. Sommerdijk, *J. Am. Chem. Soc.*, 2012**,** **134**, 1367; (*d*) H. Uchiyama and H. Imai, *Cryst. Growth Des.*, 2010, **10**, 1777; (*e*) B. Hu, L. H. Wu, S. J. Liu, H. B. Yao, H. Y. Shi, G. P. Li and S. H. Yu, *Chem. Commun.*, 2010, **46**, 2277; (*f*) D. Hu, X. Kong, K. Mori, Y. Tanaka, K. Shinagawa and Q. Feng, *Inorg. Chem.*, 2013, **52**, 10542; (*g*) S. S. Liu, D. K. Ma, Y. Q. Zhang, P. Cai, X. A. Chen and S. M. Huang, *CrystEngComm*, 2012, **14**, 2899; (*h*) A. Querejeta-Fernandez, J. C. Hernandez-Garrido, H. X. Yang, Y. L. Zhou, A. Varela, M. Parras, J. J. Calvino-Gamez, J. M. Gonzalez-Calbet, P. F. Green and N. A. Kotov, *ACS Nano*, 2012, **6**, 3800.

8 (*a*) J. Zhuang, X. Yang, J. Fu, C. Liang, M. Wu, J. Wang and Q. Su, *Cryst. Growth Des.*, 2013, **13**, 2292; (*b*) S. L. Zhong, Y. Lu, M. R. Gao, S. J. Liu, J. Peng, L. C. Zhang and S. H. Yu, *Chem. Eur. J.*, 2012, **18**, 5222; (*c*) L. Zhou, D. S. Boyle and P. O'Brien, *J. Am. Chem. Soc.*, 2008, **130**, 1309; (*d*) Y. Liu, Y. Zhang, H. Li and J. Wang, *Cryst. Growth Des.*, 2012, **12**, 2625; (*e*) C. Lausser, Michael U. Kumke, M. Antonietti and H. Cölfen, *Z. Anorg. Allg. Chem.*, 2010, **636**, 1925.

9 (*a*) R. Q. Song and H. Cölfen, *CrystEngComm*, 2011, **13**, 1249; (*b*) S. F. Chen, J. H. Zhu, J. Jiang, G. B. Cai and S. H. Yu, *Adv. Mater.*, 2010, **22**, 540; (*c*) S. F. Chen and S. H. Yu, *Chin Sci. Bull.*, 2009, **54**, 1854.

10 H. Nishizawa, K. Okumoto and T. Mitsushio, *J. Solid State Chem.*, 1991, **92**, 370.

11 (*a*) B. Q. Liu, K. Guo, J. Wang, Z. J. Zhang, Y. Tao, Y. Huang and J. T. Zhao, *Mater. Lett.*, 2013, **100**, 245; (*b*) T. Y. Sun, D. Q. Zhang, X. F. Yu, Y. Xiang, M. Luo, J. H. Wang, G. L. Tan, Q. Q. Wang and P. K. Chu, *Nanoscale*, 2013, **5**, 1629.

12 (*a*) R. A. Zehnder, D. L. Clark, B. L. Scott, R. J. Donohoe, P. D. Palmer, W. H. Runde and D. E. Hobart, *Inorg. Chem.*, 2010, **49**, 4781; (*b*) Q. Mu, T. Chen and Y. Wang, *Nanotechnology*, 2009, **20**, 345602; (*c*) J. Liang, R. Ma, F. Geng, Y. Ebina and T. Sasaki, *Chem. Mater.*, 2010, **22**, 6001; (*d*) Q. Zhu, J. G. Li, C. Zhi, X. Li, X. Sun, Y. Sakka, D. Golberg and Y. Bando, *Chem. Mater.*, 2010, **22**, 4204.

13 (*a*) F. Geng, Y. Matsushita, R. Ma, H. Xin, M. Tanaka, N. Iyi and T. Sasaki, *Inorg. Chem.*, 2009, **48**, 6724; (*b*) F. Wang, Y. Zhang, X. P. Fan, M. Q. Wang, *Nanotechnology*, 2006, **17**, 1527; (*c*) X. He and B. Yan, *J. Mater. Chem. C*, 2013, **1**, 3910; (*d*) X. He and B. Yan, *J. Mater. Chem. C*, 2014, **2**, 2368; (*e*) A. F. Kirby, F. S. Richardson, *J. Phys. Chem.*, 1983, **87**, 2557; (*f*) M. Banski, A. Podhorodecki, J. Misiewicz, M. Afzaal, A. L. Abdelhady and P. O'Brien, *J. Mater. Chem. C*, 2013, **1**, 801; (*g*) P. A. Tanner, *Chem. Soc. Rev.*, 2013, **42**, 5090.

14 X. Rao, T. Song, J. Gao, Y. Cui, Y. Yang, C. Wu, B. Chen and and G. Qian, *J. Am. Chem. Soc.*, 2013, **135**, 15559.

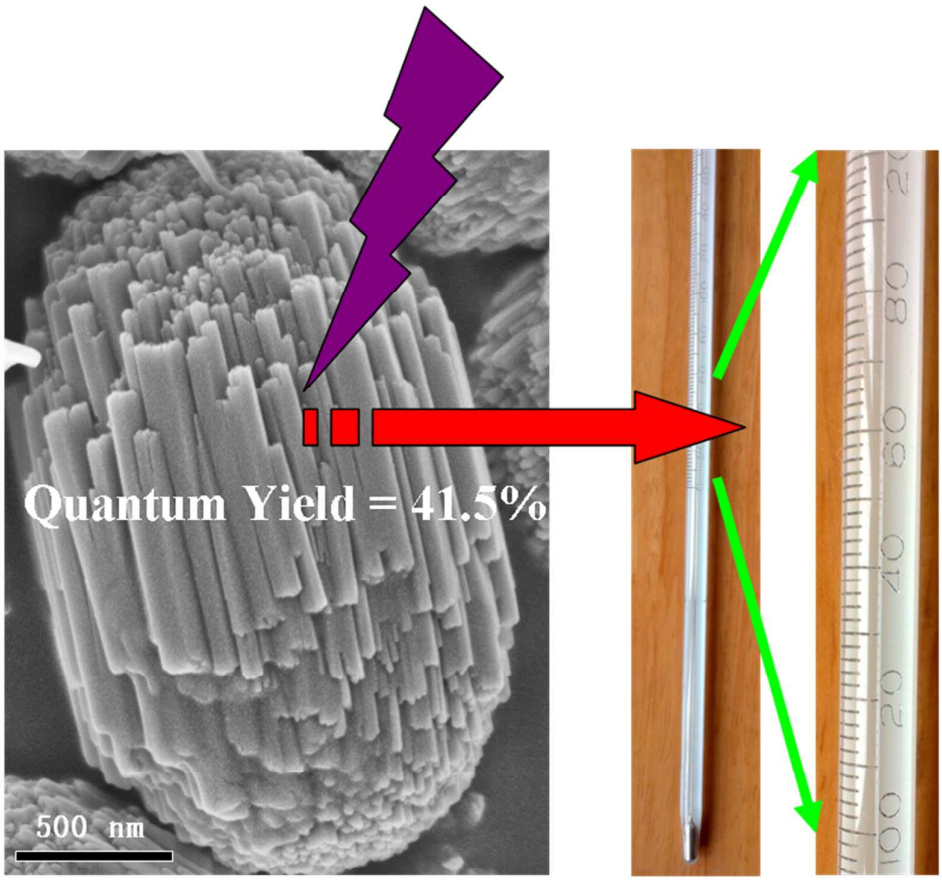

Luminescent Mesocrystal for Sensing Temperature

Here, fluorine-containing monodisperse mesocrystals constructed by nanorods was synthesized via an additive-free hydrothermal route. Eu^{3+} was successfully incorporated into yttrium hydroxide fluoride host lattice, which were supported by the facts that the reflection peaks slightly shifted towards smaller angles upon elevating Eu^{3+} content and the sample exhibits red emission after introducing Eu^{3+}. Especially, Eu^{3+}-activated mesocrystals exhibited higher red-emitting luminescence and improved efficiency, which is believed to be ascribed to the combined effects including high phase purity, well-defined facets, and highly uniform morphologies.